



Research Note

Improving thermal performance of a solar thermal/desalination combisystem using nanofluid-based direct absorption solar collector

M. Karami* and S.S. Nasiri Gahraz

Department of Mechanical Engineering, Faculty of Engineering, Kharazmi University, Mofatteh Ave., Tehran, P.O. Box 15719-14911, Iran.

Received 21 May 2021; received in revised form 7 August 2021; accepted 25 October 2021

KEYWORDS

Solar combisystem;
Direct absorption solar collector;
Nanofluid;
Humidification-dehumidification desalination unit;
Hot-dry climate;
Economic analysis.

Abstract. Depletion of freshwater resources and reduced rainfall in arid regions lead to water scarcity, which is exacerbated by population and urbanization growth. This study proposes a small-scale solar thermal/seawater desalination combisystem using a nanofluid-based direct absorption solar collector and a humidification and dehumidification desalination unit to meet the domestic hot water, space heating, and fresh water needs of a residential building. The dynamic simulation of the system performance in the hot-dry climate zone is done using the TRNSYS-MATLAB co-simulator. The results show that the use of the proposed combisystem reduces the annual energy consumption by 94.3% and 17%, respectively, for the provision of domestic hot water and space heating requirements. The supply of freshwater demand ranges from 11.3% to 100%. In addition, freshwater production decreased by an average of 18%. In the case of flat-panel solar collectors, the fraction of solar energy used for domestic hot water and space heating needs was reduced by 3.7% and 1.7%, respectively, compared with nanofluid-based direct absorption solar collectors. The payback period using nanofluid-based direct absorption and flat plate solar collectors are 6.4 and 7.8 years, respectively.

© 2022 Sharif University of Technology. All rights reserved.

1. Introduction

The significant advantages of renewable energies over fossil fuels, such as the reduction of CO₂ emissions and other types of air pollution, the reduction of reliance on imported fuels, and the economic growth and development, have resulted in a global trend to meet energy demand with renewable energy sources. Among the various renewable technologies, the Solar Combisystem (SCS), which supplies both Domestic Hot Water (DHW) and Space Heating (SH) loads of

the buildings, plays a key role in reducing building energy consumption. Therefore, scholars have recently been motivated to investigate the thermal performance of the SCSs. For instance, Mehdaoui et al. [1] simulated the dynamic performance of Tunisian SCS using TRNSYS software. The results showed that the temperature difference between different rooms was 9°C and 7°C when using the floor heating with one and two active layers, respectively. Using similar software, Hazami et al. [2] studied the SCS performance in Tunisian weather conditions. The SCS supplies 20% to 40% of the energy required for SH and 40% to 70% of the energy required for DHW, according to the researchers' findings. Rey and Zmeureanu [3] optimized the selection of configuration and equipment sizing of solar combisystems and reported that the

*. Corresponding author. Tel.: +982634579600
E-mail address: karami@khu.ac.ir (M. Karami)

proposed micro-time variant multi-objective particle swarm optimization method is a non-dominated solution to decrease the life cycle cost by 29% and to increase the life cycle energy use by 72% compared with the initial design solution. Katsaprakakis and Zidianakis [4] analyzed the performance of the SCS of a school building in Crete using the optimized dimensioning and operation automation method. It is found that the annual solar fraction of the proposed system is higher than 45%. Karami and Javanmardi [5] investigated the effect of the climatic conditions on the thermal performance of an SCS using a floor heating system. They found that the annual solar fraction in hot-dry, cold-dry, moderate-humid, hot-semi-humid, and hot-humid is 74%, 61%, 47.8%, 87.9%, and 92% respectively. Englmaier et al. [6] investigated the effect of using four PCM units, each containing 200 kg of Sodium Acetate Trihydrate (SAT) composite, in a water storage tank for SCS performance. The results showed that during heat transfer from the PCM unit to the storage tank, the flow temperature was close to the PCM temperature at thermal powers up to 6 kW. Kannan et al. [7] investigated the performance of an off-grid solar combisystem using PCM thermal storage. It is concluded that the average energy saving ratio and energy saving for space heating was about 93% and 2.8 kWh, respectively. Thapa et al. [8] designed and optimized an SCS for typical single-family houses in Nepal. The results showed that the optimum collector area and tank volumes are 6 m² and 130 lit for the Terai region and 14 m² and 150–170 lit for the Hilli region, respectively. Meister and Beausoleil-Morrison [9] evaluated a building-scale SCS with a seasonal storage tank using a two-story research house in Ottawa, Canada as a case study. Due to the use of a 36 m³ buried tank, 100% and 86% of the energy required by SH and DHW, respectively, are provided by SCS.

Another application of solar energy is the desalination of brine using direct heat from the sun, resulting in the largest share of global renewable desalination capacity of 51% [10]. Solar desalination systems are widely used in areas with high solar irradiance, which are expected to experience greater water scarcity. In recent years, several studies have been conducted on the performance of combined solar thermal/desalination systems. Asim et al. [11] analyzed the combisystem performance for producing daily DHW demand of 250 lit and daily freshwater demand of 15–25 lit of a house. Using a Flat Plate Solar Collector (FPSC) with an area of 11.85 m², 16 lit freshwater and 273 lit DHW were produced using Membrane Desalination (MD) with an air gap method. They also reported that the optimum aperture areas for flat plate and evacuated tube collectors are 8.5 and 7.5 m², respectively [12]. In another similar study, Asim [13] also found that 41.3%

and 18% of the total solar energy yield (31.3 kWh) was used for Distilled Water (DW) (0.804) and DHW production, respectively. Calise et al. [14] examined the seawater desalination performance of the system using linear Fresnel (LFR) and evacuated solar collectors using a dynamic simulation of a solar polygeneration system using ETC. They reported that the percentage of solar energy used to produce fresh water using ETC varied from 15% to 20%, and during certain winter months when ETC was used, the percentage was zero. In the following study, they found that a polygeneration system including the MED subsystem met 59% of the freshwater demand of the small Mediterranean island of Favignana [15]. Kumar and Martin [16] studied DW and DHW production in the UAE using a novel combisystem. They noted that the maximum DW yield of the stand-alone distillation system was 4.5 kg/h, which was 36% higher than the yield of combisystem (3.1 kg/h).

The humidification-dehumidification (HDH) process is one of the desalination methods that can produce DW utilizing solar thermal energy. This method is based on the fact that air can carry a lot of water vapor. When air comes in contact with salt water, some of the water evaporates and is absorbed by the air. This steam can be distilled and recycled by passing from cold surfaces to produce DW. Tariq et al. [17] revealed that by introducing a novel air saturator, they were able to produce 30% more freshwater than a conventional HDH system. Rahimi-Ahar et al. [18] conducted an experimental and thermodynamic analysis of a solar-assisted vacuum HDH desalination plant and found that at the optimal water to air mass flow rate ratio and minimum humidifier pressure, the maximum desalination rate of 1200 mL/h.m² is achieved. Zhao et al. [19] used 42 m² Parabolic Trough Collectors (PTC) as the energy source of a four-stage cross flow HDH with direct contact dehumidifier. The results indicated that the proposed system has a higher water yield per unit volume (34.1 kg/m³h) and lower pure water yield cost (3.86 \$/ton) in comparison with conventional HDHs. In an interesting experimental study, Rajaseenivasan and Srithar [20] integrated the HDH system with a dual-purpose solar collector to heat both water and air during the distillation process. It is found that the maximum DW of 15.23, 14.14, and 12.36 kg/m².d is produced for the concave, convex, and conventional systems, respectively. They concluded that, depending on the PVT configuration and environmental conditions, DW production is maximized at the highest possible brine flow rate.

The literature review illuminates that the thermal performance of solar thermal/desalination combisystems has not been yet assessed using a Nanofluid-based Direct Absorption Solar Collector (NDASC) [22]. In addition, the performance of the solar ther-

mal/desalination combisystems for small residential buildings using HDH desalination systems has not been investigated. Therefore, the primary goal of this article is to look into the feasibility and efficiency of integrating an HDH desalination system with an SCS for small-scale DW production using an NDASC as a solar collector. The thermal performance of the proposed combisystem is evaluated using the TRNSYS dynamic simulation software. Furthermore, the economic analysis of the proposed HDH-SCS is performed using the Life Cycle Cost (LCC) method.

2. System descriptions

The thermal performance of an HDH-SCS, which supplies the DHW, SH, and freshwater demands of a single-floor house with a 100 m² area, is explored in this research as a case study building. The house is located in a hot and dry climate zone (City of Tehran, Iran, Latitude 35.68, Longitude 51.4). Table 1 shows the characteristics of the case study building.

In Figure 1, a schematic diagram of HDH-SCS is illustrated. The working fluid of the solar cycle, i.e. water or nanofluid, passes through the NDASC or FPSC and enters Diverter 1 (FD1) with increased temperature. The DHW tank receives the portion of the collector working fluid that is necessary for DHW supply. The rest of the collector working fluid goes to the FD2 and then to the SH tank during the colder months and transfers its heat to the tank water. The heated water goes to the auxiliary boiler as preheated water and is heated to the desired setpoint temperature. In warm months, when there is no need

for SH, the collector working fluid from FD2 enters the DW tank and heats the outlet saline water from the dehumidifier (DHUM). Hot brine enters the humidifier (HUM) and is sprayed into the air passing through, causing an increase in air temperature and humidity. The moist hot air enters the DHUM, and the water vapor in the air condenses due to indirect contact with the inlet brine, resulting in DW. The outlet working fluid from the DW and SH tanks enters Mixing Valve 1 (MV1), where it is mixed with the outlet working fluid from the DHW tank in MV2 before being returned to the solar loop to repeat the cycle.

2.1. System dynamic modeling

In this paper, the dynamic simulation of HDH-SCS is performed using TRNSYS, a transient software for real-time simulation of energy systems that contains a large library of built-in components and open-source models. TRNSYS modeling of the system allows for dynamic computation and integration of output data for each system component, such as power, mass flows, temperature, and so on. Figure 2 shows the TRNSYS modeling of the HDH-SCS. In the model, various types have been selected for simulating the behavior of the system components. Type 109 was used to read weather data from the Typical Meteorological Year (TMY) files and calculate the solar radiation in different directions. Psychrometric properties such as dew point, relative humidity, etc. are calculated by Type 33. Type 1b, a quadratic efficiency model with incidence angle modification, was used to model the FPSC. Because there is no component for the NDASC in TRNSYS standard component library, a new component is developed by writing code in MATLAB-R2015b and then linking the MATLAB code to the TRNSYS simulation program using Type 155.

Types 4 and 3b were used to model the storage tanks and pumps. The volumes of the DHW, SH, and DW tanks are 300 liters, 800 liters, and 200 liters respectively. To simulate a 15 kW auxiliary boiler with an efficiency of 78%, Type 700 was used. The daily DHW demand is simulated using Type 14b, whose profile is given in Figure 3 [23]. The other TRNSYS components used in the simulations are Type 11 and Type 11h, which simulate a flow diverter and a mixing valve, respectively. System controllers (Type 2b) are used to control the flow rate of the collectors and the storage tanks. In addition to NDASC, there is also no TRNSYS type for the HDH desalination system; therefore, it is modeled by MATLAB and connected to TRNSYS using Type 155.

Using the results of the simulation, the performance indicators of the HDH-SCS can be determined. The DHW solar fraction (SFDHW) and SH solar fraction (SFSH) is defined as the ratio of energy supplied by solar energy to the required energy, given by the

Table 1. Case study building specifications.

Parameter	Value
Floor area	100 m ²
Overall heat transfer coefficient of 0.04 W/(m ² K) external walls	
Overall heat transfer coefficient of 0.14 W/(m ² K) roof	
Overall heat transfer coefficient of 1.25 W/(m ² K) windows	
Inside set point temperature	22 °C
Window-to-Wall Ratio (WWR)	30%
Occupants	4 persons
Occupant activity level	Seated, light work
Natural ventilation	1 ACH
Infiltration	0.16 ACH
Artificial lighting	5 W/m ²
Domestic hot water demand per 50 l person	
Domestic hot water temperature	60 °C
Freshwater demand per person	150 l

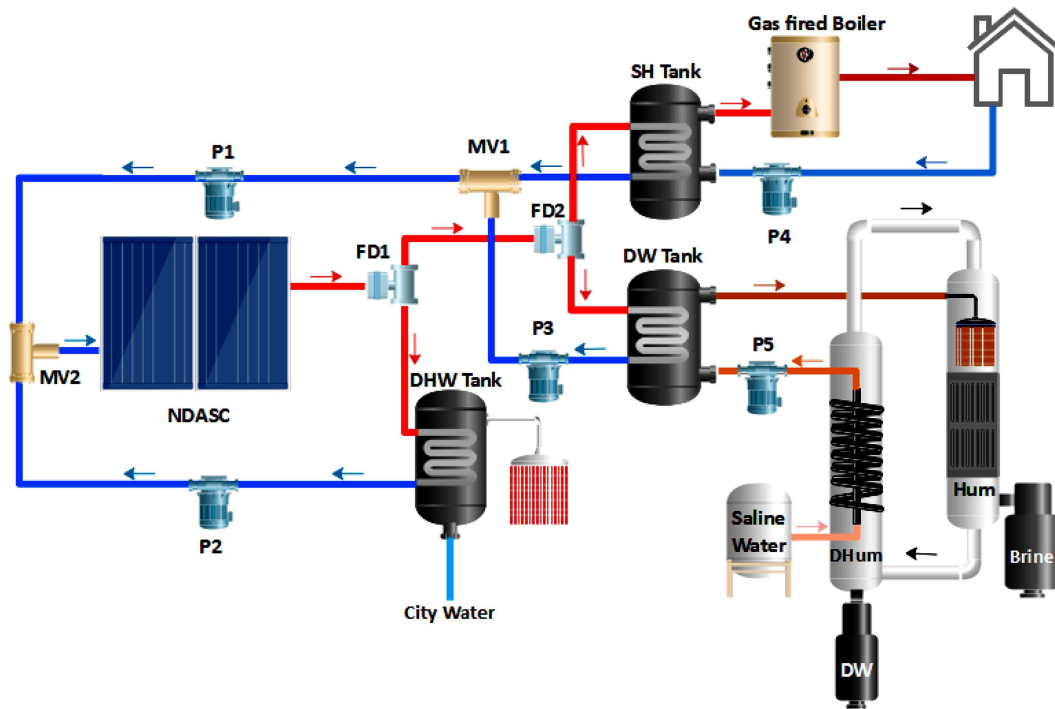


Figure 1. Schematic of the proposed HDH-SCS.

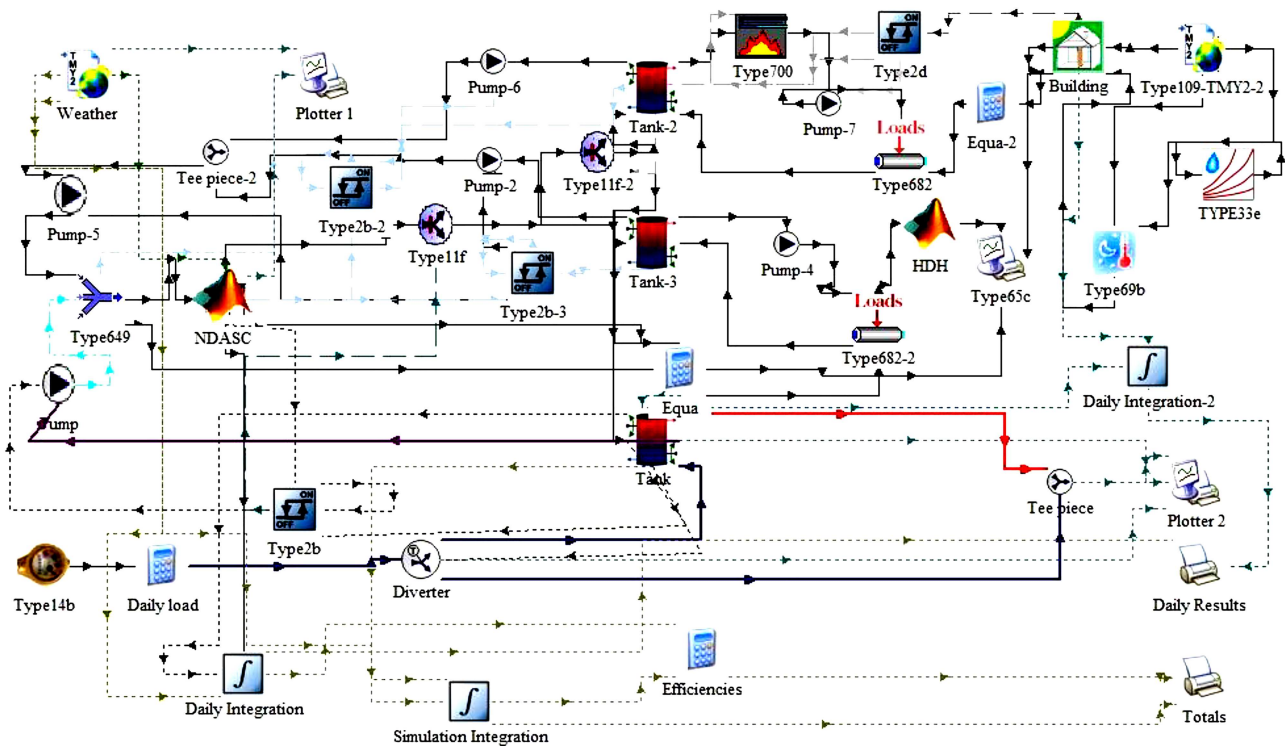


Figure 2. Descriptive diagram of TRNSYS model of HDH-SCS.

following relations:

$$SF_{DHW} = 1 - \frac{Q_{aux,DHW}}{Q_{DHW,demand}}, \quad (1)$$

$$SF_{SH} = 1 - \frac{Q_{aux,SH}}{Q_{SH,demand}}. \quad (2)$$

2.1.1. NDASC modeling

Solar radiation is absorbed directly by the nanofluid as the working fluid in NADSC, whereas in conventional collectors, solar radiation is absorbed indirectly by a surface absorber. The schematic of the NDASC, which

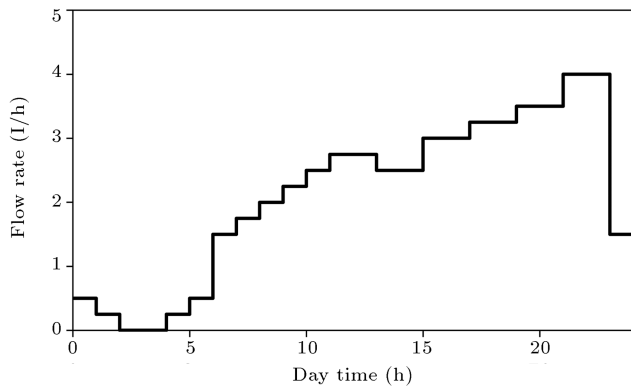


Figure 3. Hourly DHW consumption profile [23].

has an aperture area of 2 m × 1 m and a channel height of 1 cm, is presented in Figure 4.

The collector useful heat gain (\dot{Q}_u), which is used for supplying the required thermal energy of the proposed system, is calculated using the following relation:

$$\dot{Q}_u = \dot{m}_{nf} c_{p,nf} (T_{out} - T_{in}), \quad (3)$$

where \dot{m}_{nf} and $c_{p,nf}$ are the mass flow rate and the heat capacity of diamond nanofluid.

To calculate the useful energy gain, the collector outlet temperatures should be calculated by solving the conservation equations governing the performance of the NDASC. It should be noted that the back and walls of the collector are considered the adiabatic boundary condition. The nanoparticles are stably suspended in the base fluid and because of the surface-to-volume ratio of the nanoparticles, they have the same temperature as the base fluid [24].

By considering the above assumptions, the mass, momentum, and energy conservation equations for two-dimensional, steady-state, incompressible flow inside the collector are given as [25]:

$$\frac{\partial u}{\partial x} + \frac{\partial v}{\partial y} = 0, \quad (4)$$

$$\rho \left(u \frac{\partial u}{\partial x} + v \frac{\partial u}{\partial y} \right) = -\frac{\partial P}{\partial x} + \mu \left(\frac{\partial^2 u}{\partial x^2} + \frac{\partial^2 u}{\partial y^2} \right), \quad (5)$$

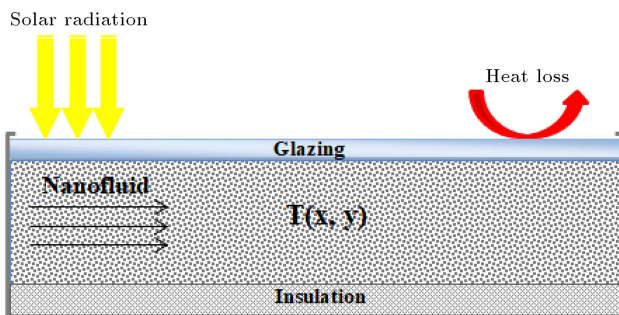


Figure 4. Schematic of NDASC.

$$\rho \left(u \frac{\partial v}{\partial x} + v \frac{\partial v}{\partial y} \right) = -\frac{\partial P}{\partial y} + \mu \left(\frac{\partial^2 v}{\partial x^2} + \frac{\partial^2 v}{\partial y^2} \right), \quad (6)$$

$$\rho c_P \left(u \frac{\partial T}{\partial x} + v \frac{\partial T}{\partial y} \right) = \left(\frac{\partial}{\partial x} \left(k \frac{\partial T}{\partial x} \right) + \frac{\partial}{\partial y} \left(k \frac{\partial T}{\partial y} \right) \right) - \nabla \cdot q_r, \quad (7)$$

where q_r is a radiation source term that takes into account the absorption of solar energy by the nanofluid [26].

The volumetric heat transfer due to radiation, which is the last term on the right-hand side of the Eq. (7), is given by [26]:

$$\nabla \cdot q_r(y) = 4 \int_{\lambda} K_{a\lambda} \left[I_b(\lambda, y) - \frac{1}{4\pi} \int_{\omega_i=0}^{4\pi} I_{\lambda}(\lambda, y, \omega) d\omega_i \right] d\lambda, \quad (8)$$

where λ is the wavelength, $K_{a\lambda}$ is the spectral absorption coefficient, and I_b is the blackbody intensity given by the Planck function. It is assumed that the radiation intensity variation occurs in one dimension along the y-direction; therefore, the spectral intensity (I_{λ}) is obtained by solving the Radiative Transfer Equation (RTE):

$$\frac{dI_{\lambda}}{dy} = - (K_{a\lambda} + K_{s\lambda}) I_{\lambda}(y) + K_{a\lambda} I_{\lambda b}(y) + K_{s\lambda} / 4 \int_{\omega_i=0}^4 I_{\lambda}(y, \omega_i)(\omega, \omega_i) d\omega_i, \quad (9)$$

where $K_{s\lambda}$ is the spectral scattering coefficient; $I(y, \omega) \dots (\omega, \omega)$ are the scattering phase function and the spatial angle, respectively. The sum of absorption and scattering coefficients is called spectral extinction coefficient (K_e). The scattering coefficient ($K_{s\lambda}$) can be ignored at the nanometer scale according to Rayleigh scattering [26]. Regarding the assumptions, the intensity distribution within the solar collector is obtained using the following equation:

$$\frac{dI_{\lambda}}{dy} = -K_{a\lambda} I_{\lambda}(y) + K_{a\lambda} I_{\lambda b}(y). \quad (10)$$

The emitted radiation can be determined using Planck's blackbody relation given in Eq. (14) [27]:

$$I_{\lambda b}(\lambda, T(x, y)) = \frac{2hc^2}{\lambda^5 \left[\exp \left(\frac{hc}{\lambda k_B T} \right) - 1 \right]}, \quad (11)$$

where h , k_B , and c are Planck's constant, Boltzmann's constant, and the speed of light in a medium, respectively. By solving Eqs. (4) to (7) using the following boundary conditions, the pressure, velocity, and temperature distributions in the collector are obtained:

$$x = 0, \quad 0 < y < H \rightarrow T(0, y) = T_{in}, \quad u(0, y) = U_{in}, \quad (12)$$

$$y = 0, \quad x > 0 \rightarrow -k \left. \frac{\partial T}{\partial y} \right|_{y=0} = (1 - \tau_{g,\lambda}) G_T - h(T_{amb} - T_g), \quad (13)$$

$$y = H, \quad x > 0 \rightarrow \left. \frac{\partial T}{\partial y} \right|_{y=H} = 0, \quad (14)$$

where h is the combined convection and radiation heat transfer coefficient of the glass upper surface; T_{in} , U_{in} , and G_T are the constant temperature and velocity of the inlet fluid, and the solar incident radiation on the tilted collector, respectively. In this study, the collector is mounted at a tilt angle in the latitude of Tehran to receive maximum solar energy [26]. T_g and $\tau_g = 90\%$ are the temperature and transmissivity of the glass, respectively.

In this study, the fully implicit finite difference method is used to solve the governing equations and boundary conditions. First, the two-dimensional mass and momentum equations are solved using the SIMPLE method to determine the velocity distribution in the collector [28]. Then, the energy equation is solved using the velocity distribution. Because the emission term couples the RTE and the energy equation, an iterative solution method is employed to calculate the blackbody emission term in Eq. (14) by guessing the temperature profile. Then, Eq. (13) is solved to obtain the intensity distribution, which is used in the energy equation to determine the temperature profile. If the new calculated temperatures have a little difference with the initial guess of the temperature profile, the solution is converged; otherwise, the new temperature profile is used to update the blackbody emission term and the solution is repeated to achieve convergence.

To validate the results of the NDASC model, the measured and calculated efficiency of the NDASC are compared. As can be seen in Figure 5, the experimental

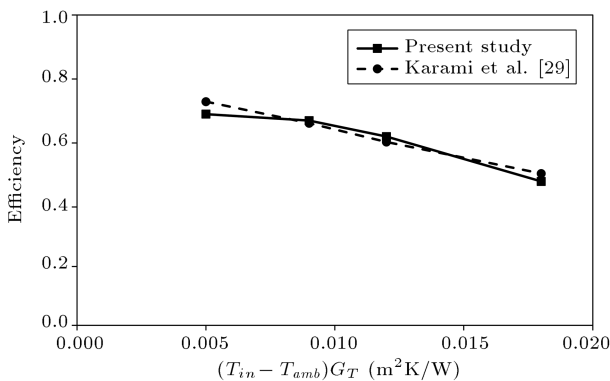


Figure 5. Comparison of the experimental and numerical efficiency of NDASC.

and numerical results were in good agreement with a maximum error of 4% [29].

2.2.1.1. Nanofluid preparation and optical properties

In this study, diamond nanoparticles (10 nm in diameter, 98.3% average purity) produced by Luoyang Tongrunjingnuo Technology are selected as the working fluid of NDASC in an aqueous suspension with a concentration of 0.001 wt%. The nanofluid preparation method is a two-step procedure in which diamond nanoparticles are first dispersed in deionized water (the base fluid) to form the nanodiamond-water nanofluid, and then the suspension is stirred using an ultrasonic processor (UP400S). After sonicating the suspension for 15 minutes, a surfactant called Gum Arabic (GA) is added to improve nanofluid stability, and the sonication procedure is repeated for yet another 30 minutes. More details about the nanofluid materials and preparation can be found in [29].

The transmittance and extinction coefficient of the prepared nanofluid are experimentally determined using UV-Vis-NIR spectrophotometer (Cary 5, Varian Inc., USA) as shown in Figure 5. The extinction coefficient of the nanofluid is calculated using Beer-Lambert law ($T(\lambda) = e^{-K_e \lambda H}$), in which $T(\lambda)$ is the nanofluid transmittance and H is the length of the light passing through the sample. It is assumed that the no incident radiation collector reaches the bottom surface, because the transmittance of the nanofluid is nearly zero, as shown in Figure 6. It should be noted that the thermophysical properties of the nanofluid are considered as the base fluid due to the very low concentration of the nanofluid [29].

2.1.2. HDH modeling

Figure 7 shows the components of a Closed Air Open Water (CAOW) HDH desalination system for producing DW, which is used in this study. For modeling the HDH performance, the mass and energy conservation equations are written as follows:

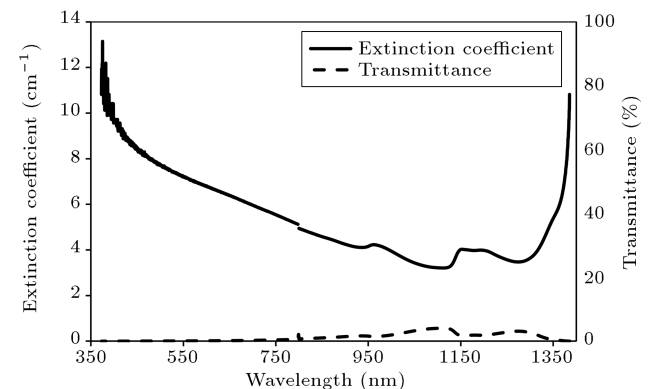


Figure 6. Spectral transmittance and extinction coefficient of diamond nanofluid with concentration of 0.001 wt% [29].

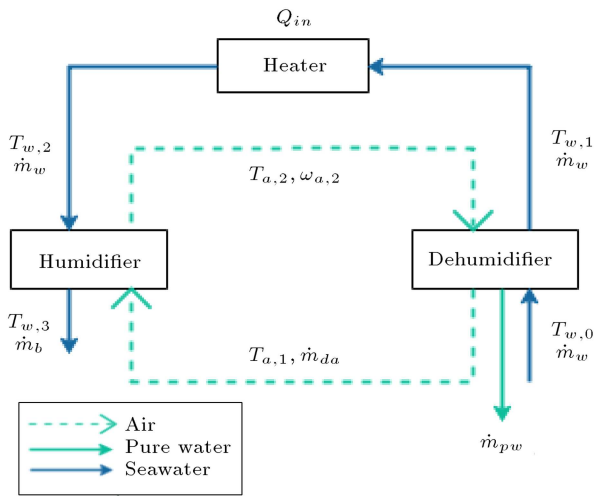


Figure 7. Schematic of a CAOW-HDH desalination system.

Dehumidifier [30]:

$$\dot{m}_{pw} = \dot{m}_a(\omega_{a,2} - \omega_{a,1}), \tag{15}$$

$$\dot{m}_w(h_{w,1} - h_{w,0}) + \dot{m}_{pw}h_{pw} = \dot{m}_a(h_{a,2} - h_{a,1}). \tag{16}$$

Humidifier [30]:

$$\dot{m}_w - \dot{m}_a(\omega_{a,2} - \omega_{1,a}) = \dot{m}_b, \tag{17}$$

$$\dot{m}_a(h_{a,1} - h_{a,2}) = \dot{m}_bh_{w,3} - \dot{m}_wh_{w,2}. \tag{18}$$

It is assumed that the humidifier and dehumidifier are insulated.

The heat transfer from the collector to the fluid is obtained by using the following equation:

$$\dot{Q}_{heater} = \dot{m}_wc_{p,w}(T_{w,2} - T_{w,1}). \tag{19}$$

In this paper, the enthalpy and relative humidity of the air are calculated as a function of the air flow temperature using the following relations [31]:

$$h = 0.005853T^3 - 0.497T^2 + 19.87T - 207.61, \tag{20}$$

$$\omega = 2.19 \times 10^{-6}T^3 - 1.85 \times 10^{-4}T^2 + 7.06 \times 10^{-3}T - 0.077. \tag{21}$$

There are five unknowns ($T_{a,1}, T_{a,2}, T_{w,1}, T_{w,2}, T_{w,3}$) in Eqs. (16), (18), and (19); therefore, for solving the equations, the effectiveness of the heat exchanger can be used as the supplementary equations and are defined as [30]:

$$\varepsilon = \frac{\Delta \dot{H}}{\Delta \dot{H}_{max}}, \tag{22}$$

where $\Delta \dot{H}$ is the enthalpy changes of cold or hot fluid

and $\Delta \dot{H}_{max}$ is the maximum enthalpy change that the fluid can achieve.

Since humidifiers and dehumidifiers act as heat exchangers, the efficiencies of humidifiers and dehumidifiers, respectively, can be calculated using the following relationship:

$$\varepsilon_H = \max\left(\frac{h_{a,out} - h_{a,in}}{h_{a,out,ideal} - h_{a,in}}, \frac{h_{w,in} - h_{w,out}}{h_{w,in} - h_{w,out,ideal}}\right), \tag{23}$$

$$\varepsilon_D = \max\left(\frac{h_{a,in} - h_{a,out}}{h_{a,in} - h_{a,out,ideal}}, \frac{h_{w,in} - h_{w,out}}{h_{w,in} - h_{w,out,ideal}}\right). \tag{24}$$

The equations are solved using the iterative solution method with the inputs including the inlet water temperature, the air temperature, the water flow rate, the air flow rate, and the inlet heat rate. In calculating the ideal enthalpy difference, it is assumed that there is no temperature difference between the inlet and outlet flows of the chamber. In other words, $T_{in,w} = T_{a,out,ideal}$ and $T_{in,a} = T_{w,out,ideal}$. It is also assumed that the outlet water temperature of the humidifier is the average of the inlet and outlet air temperatures and that the air at the outlet of the humidifier is saturated. Figure 8 shows the flowchart of the HDH modeling process.

A comparison of the results of the HDH model is shown in Figure 9, where the measured and calculated Gained Output Ratio (GOR) of the HDH is compared at different brine inlet temperatures. The GOR is defined as:

$$GOR = \frac{\dot{m}_{fw} \cdot h_{fg}}{\dot{Q}_{in}}, \tag{25}$$

where \dot{m}_{fw} , h_{fg} , and \dot{Q}_{in} are the freshwater mass flow rate, the evaporation enthalpy, and the inlet thermal power to the HDH, respectively. As shown in Figure 9, the experimental and numerical results are in good agreement with a maximum error of 7% [30].

3. Results and discussion

Figure 10 reveals the monthly average solar radiation and ambient temperature in Tehran. As observed, the maximum ambient temperature is 30.9°C in July and its minimum is 2.46°C in January. The maximum solar radiation is about 730 W/m² in August.

In Figure 11, the monthly variations of the DHW energy demand, supply, auxiliary energy demand, and SFDHW are plotted. Figure 9 shows that from May to October, the SFDHW can be increased by more than 90% by using FPSC. From November to April, the SFDHW varies between 75% and 88.5%. It is worth noting that auxiliary energy is necessary in all months, even in months where the supplied energy is

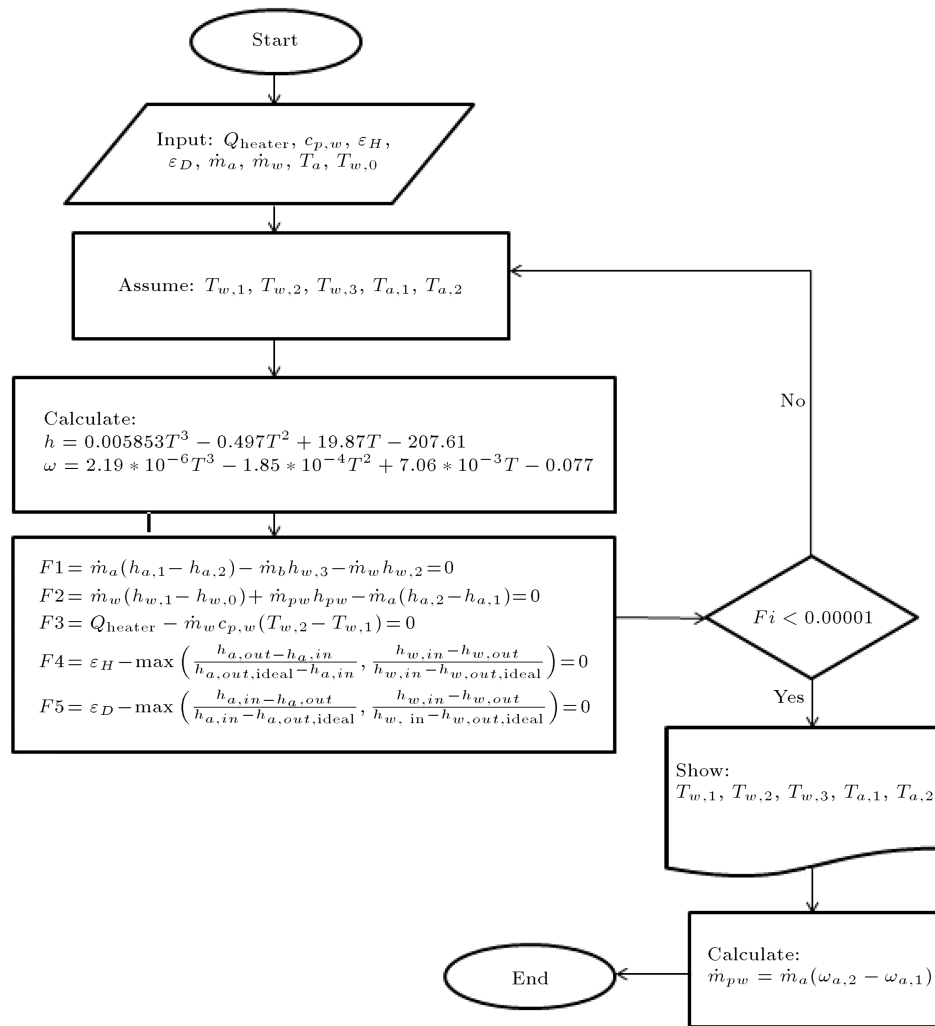


Figure 8. Flowchart of the HDH modeling process.

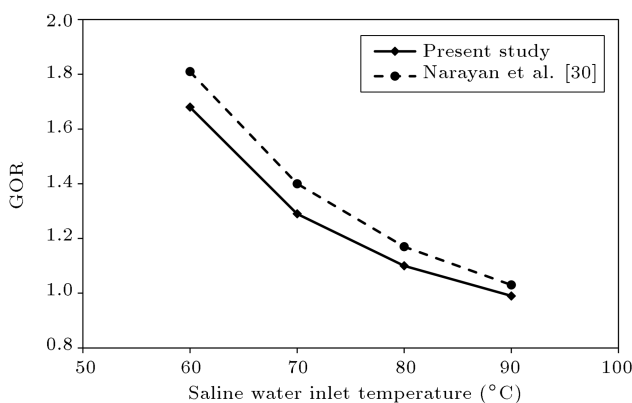


Figure 9. Comparison of the experimental and numerical GOR.

more than the required energy, such as July, August, and September. This is because the tank temperature decreases at night or on cloudy days.

Due to increasing solar energy absorption, the system SFDHW increases employing NDASC instead of FPSC, as shown in Figure 11(b), resulting in an

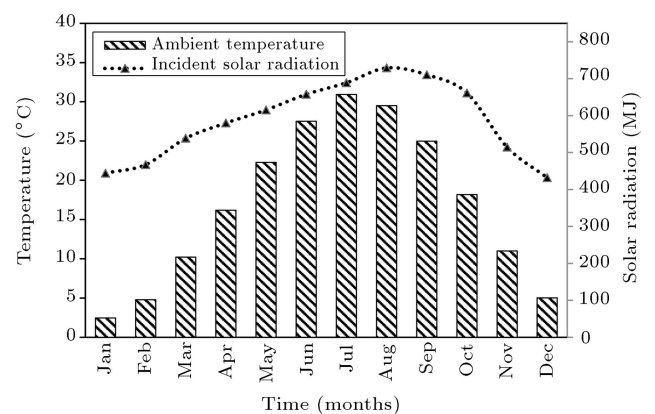


Figure 10. Monthly solar radiation and monthly average air temperature in Tehran.

SFDHW of 100% from June to September. The maximum and minimum enhancement of SFDHW is obtained in January and August, which are 6.3% and 1.1%, respectively. This suggests that the use of NDASC can improve the thermal performance of the

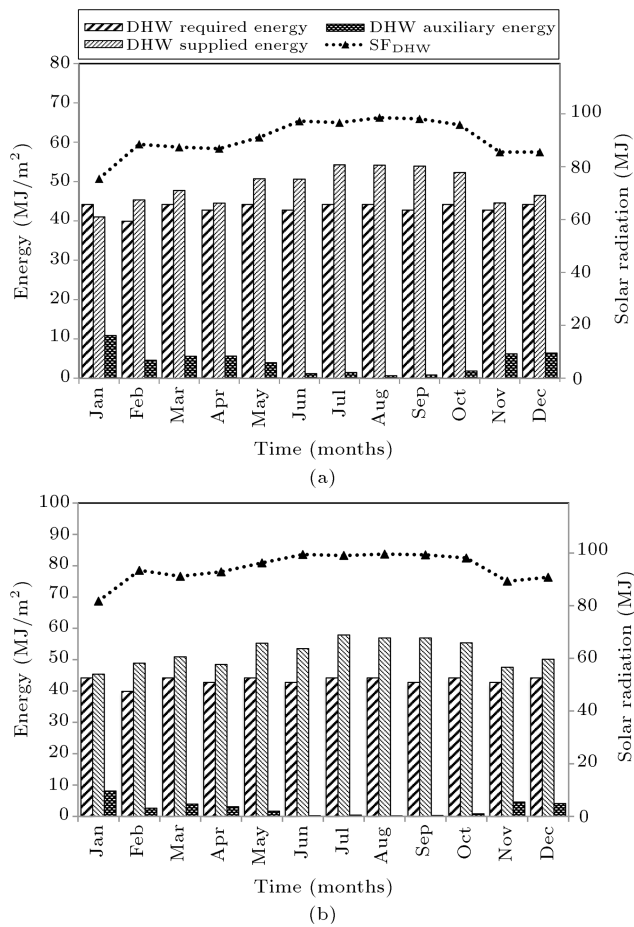


Figure 11. Monthly changes in DHW energy demand, supply, auxiliary energy demand, and solar fraction using: (a) FPSC and (b) NDASC.

combisystem, especially in cold seasons when solar radiation is low. The annual solar fraction for DHW was 90.5% and 94.3% using FPSC and NDASC, respectively.

Figure 12 shows the monthly changes in SH demand, supply and auxiliary energy demand, and SFSH. As shown in Figure 12(a), the SFSH in January, February, March, November, and December were 18.2%, 20.0%, 11.0%, 13.2%, and 13.97%, respectively. In October, April, and May, all the energy required by the SH is supplied by auxiliary energy, since the thermal energy of the SH is required at night. According to the results shown in Figure 12(b), the auxiliary energy required with NDASC increased from 0.9% in March to 2.4% in January compared with FPSC. The annual SFSH is 15.2% and 17.5% using FPSC and NDASC, respectively.

In the proposed HDH-SCS, when the energy needs for DHW and SH are met, the excess heat is used to produce the DW using the HDH desalination system. In Figure 13, the monthly variation of the produced DW by the system is shown. As can be seen, using two collectors, the produced DW increases by

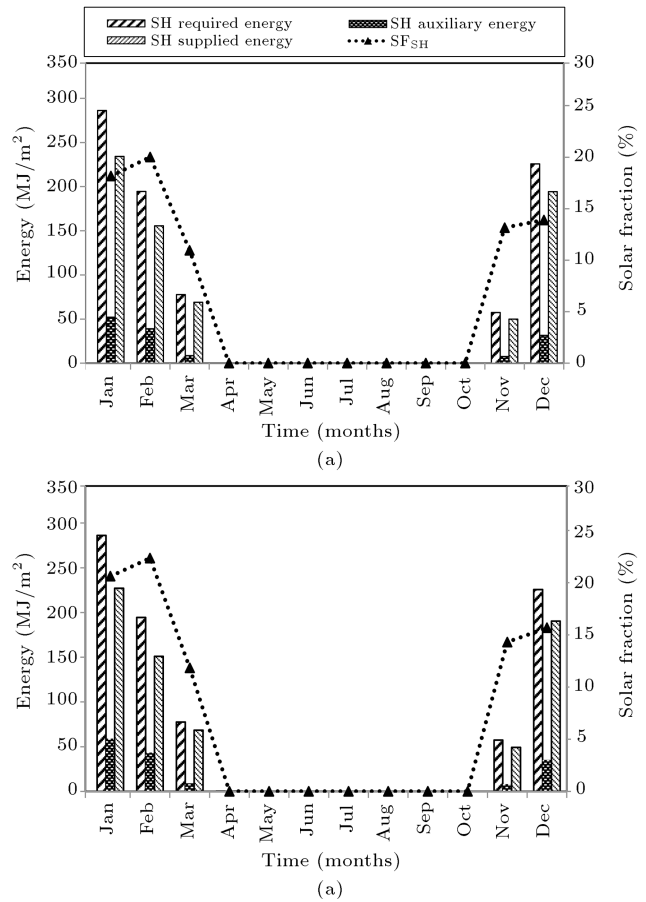


Figure 12. Monthly changes in SH energy demand, supply, solar fraction, and auxiliary energy demand using: (a) FPSC and (b) NDASC.

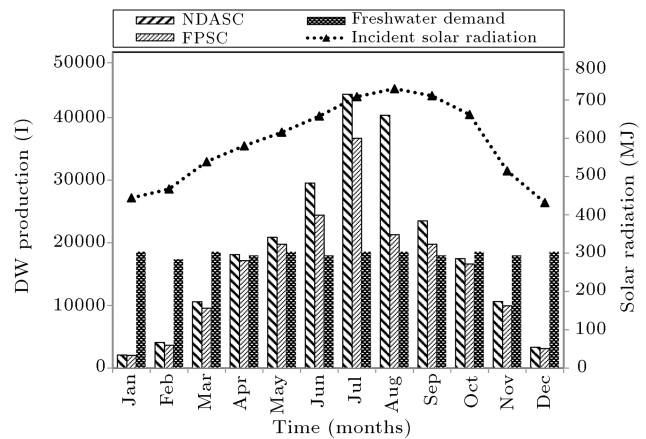


Figure 13. Monthly variations of freshwater demand and DW production.

increasing the incident solar radiation. Using FPSC and NDASC, the maximum DW of about 36,700 l and 43,700 l respectively, is produced in July, while the minimum DW of 2,036.1 l and 2,092.6 l is produced in January, respectively. The annual DW produced by NDASC is 224,370 l, which is 18% higher than that produced by FPSC.

Given that the average daily freshwater demand per person is 150 liters [32], it can be concluded that the DW demand from April to September is entirely supplied by the system and the excess DW can be sold. In other months, the produced DW can provide the DW demand in the range of 11.3% in January to 93.9% in October.

4. Economic analyze

In this study, the Life Cycle Cost (LCC) method is used to analyze the economic impacts of the proposed HDH-SCS [33]. In this approach, all costs of the system over its lifetime are added up, taking into account the time value of money. The economic scenario used in this study is that no mortgage is obtained and that the full cost of the system is paid in advance. Therefore, for a solar plus auxiliary system, the LCC is estimated by the following equation:

$$\begin{aligned} \text{system cost} &= \text{initial cost} + \text{fuel cost} \\ &+ \text{parasitic energy cost} + \text{maintenance cost.} \end{aligned} \quad (26)$$

The initial cost includes the cost of equipment, design, transportation, installation, and installation space if not installed on the roof of the building. The cost of equipment includes the cost of solar collectors, storage tanks, pumps, pipes, insulation, heat exchangers, and controllers. In this study, the cost of the FPSC and NDASC are 75 and 60 $\frac{\$}{\text{m}^2}$, respectively; therefore, by considering the collector area of 18 m², the initial cost of collectors is 1350\$ and 1080\$, respectively [34]. The cost of NDASC is lower than that of FPSC due to the removal of absorber plates and absorber tubes. However, due to the use of nanofluids as working fluid, the total capital cost of NDASC is considered to be around 1.2 times that of FPSC [35]. The cost of the HDH system and the auxiliary boiler are considered 700\$ and 490\$, respectively.

The operational cost includes fuel, parasitic energy, and maintenance costs, which is considered a percentage of the initial investment cost and increases annually at a certain rate. In this study, the cost of system maintenance, initially estimated at 1% of the initial system cost, increased by 0.5% per year as the system ages [33]. It should be noted that the maintenance cost of NDASC is also considered to be 1.2 times higher than that of FPSC due to the use of nanofluids [35].

The cost of the fuel consumed by the auxiliary heater is calculated using the following relation:

$$C_{AUX} = C_{FA} \int_0^t L_{AUX} dt, \quad (27)$$

where C_{FA} is the cost rate (\$/GJ) for auxiliary fuel.

The Present Worth (PW) of the system cost is expressed as:

$$PW_n = \frac{\text{System cost} \times (1 + i)^{n-1}}{(1 + d)^n}, \quad (28)$$

where d is the market discount rate which is the reduction in the time value of money over time, and n is the number of life cycle years.

The Life Cycle Savings (LCS) is the difference between the cost of a solar system and the cost of a conventional system that works with fossil fuels:

$$\begin{aligned} \text{System savings} &= \text{fuel savings} + \text{water cost} \\ &+ \text{resale value} - \text{extra parasitic energy cost} \\ &- \text{extra maintenance cost,} \end{aligned} \quad (29)$$

where resale value is the cost to resell the system at the end of its life and is considered to be 30% of the initial cost. The total present worth of the gains from the solar system compared to the fuel-only system is also obtained using Eq. (29).

Another economic indicator, which is used for the comparison of the systems, is the payback time. It is the time to return the initial capital or the time required for the annual solar savings to become positive [33]. In this study, the period of economic analysis is equivalent to the life of the system, which is taken as 20 years. Inflation and discount rates are assumed identical to the Iran's economic indicators for 2016, which were 9.6% and 15%, respectively [36]. The government subsidizes freshwater as well as energy carriers such as natural gas and electricity in Iran; however, in this analysis, the non-subsidized global prices are considered to make the analysis more logical. The natural gas, electricity, and freshwater prices are considered 0.7715 $\frac{\$}{\text{m}^3}$, 0.15 $\frac{\$}{\text{kWh}}$ and 2.8 $\frac{\$}{\text{m}^3}$, respectively [37,38]. The annual inflation rates of natural gas, electricity, and freshwater prices are expected to be 15%, 3%, and 6%, respectively. The results of the economic analysis are listed in Table 2. As can be seen, because of the lower initial system cost and higher LCS for fuel and water costs, the payback period of the system using NDASC is about 18% lower than that of the system using FPSC. The results confirm the better performance of the proposed HDH-SCS using NDASC as a solar collector.

Table 2. Results of economic analysis.

Parameter	FPSC	NDASC
System cost (\$/m ²)	3733.5	3606
LCS for fuel cost (m ³ /year)	25586.6	27074.9
LCS for water cost (\$)	8915.4	11831.6
Payback period (year)	7.8	6.4

5. Conclusion

In this study, the performance of the HDH-SCS has been studied in the hot-dry climate zone. Using the proposed system, in addition to DHW and SH demands, the freshwater demand of the residential case study building is also met. The findings can be summarized as follows:

- The monthly SF_{DHW} of the proposed system using NDASC is larger than that using FPSC because of more solar absorption by the nanofluid. The maximum SF_{DHW} enhancement of 6.3% is achieved in January, which indicates better system performance in cold months using NDASC;
- The auxiliary energy of SH is always higher than that of DHW because most of the useful gain of the collector is allocated to the provision of DHW. In other words, SF_{DHW} is higher than SF_{SH} in all months. The maximum SF_{SH} of 20.0% is achieved by the proposed system in February. In comparison with the FPSC-based system, the SH auxiliary energy decreased 2.4% in January;
- The DW demand from April to September is completely supplied by the system. The produced DW by the proposed system could supply the DW demand in the range of 11.3% in January to 93.9% in October;
- Economic analysis using the LCC method showed a cost savings of 38,900\$ over the life of the system, with a payback period of 6.4 years;
- The system performance is enhanced by using diamond nanofluid as the working fluid of the DASC instead of the FPSC. Annual DHW and SH solar fractions increased by 3.8% and 1.8%, respectively. The annual production of DW was on average 18% higher. LCS increased by 11.3% and the payback period decreased by about 18%. It is concluded that nanofluid-based DASCs are a better choice for use as an energy source in the proposed system;
- The results show that combining a solar thermal combisystem with a thermal desalination system can prevent heat loss from the system, especially during hot seasons, and recovered heat can be used for producing DW. As a result, employing this approach aids in the remedy of people's lack of access to freshwater.

Nomenclature

C	Cost (\$)
c	Light velocity (m/s)
c_p	Specific heat (kJ/kg.K)
d	Discount rate

G_T	Total solar irradiance incident on the aperture of tilted collector (W/m^2)
H	Height (m)
\dot{H}	Enthalpy rate (W)
h	Specific enthalpy (J/kg)
h	Heat transfer coefficient ($W/m^2.K$)
I	Intensity (W/sr)
i	Inflation rate
$K_{a\lambda}$	Absorption coefficient (m^{-1})
$K_{s\lambda}$	Scattering coefficient (m^{-1})
$K_{e\lambda}$	Extinction coefficient (m^{-1})
k	Thermal conductivity ($W/m.K$)
k_B	Boltzmann constant
L	Load (J)
\dot{m}	Mass flow rate (kg/s)
n	Number of years
P	Pressure (Pa)
\dot{Q}	heat transfer rate (kJ/h)
q_r	Radiative source term (W/m^2)
T	Temperature (K)
t	Time (s)
U	Velocity (m/s)
u, v	Velocity (m/s)
x, y	Coordinates (m)

Greek Symbols

ρ	Density (kg/m^3)
λ	Wavelength (m)
ε	Effectiveness
τ_g	Glass transmittance
ω	Absolute humidity (kg_w/kg_{da})
ω	Spatial angle
μ	Viscosity (kg/m.s)
Φ	Scattering phase function

Subscripts

a	Air
amb	Ambient
b	Brine
AUX	Auxiliary
D	Dehumidifier
da	Dry air
FA	Auxiliary fuel
fg	Fluid-gas
H	Humidifier
in	Inlet

<i>nf</i>	Nanofluid
<i>out</i>	Outlet
<i>pw</i>	Product water
<i>r</i>	Radiative
<i>u</i>	Useful
<i>w</i>	Water
λ	Spectral

Acronyms

DHW	Domestic Hot Water
DW	Distilled Water
FPSC	Flat Plate Solar Collector
GOR	Gain Output Ratio
NDASC	Nanofluid-based Direct Absorption Solar Collector
LCC	Life Cycle Cost
LCS	Life Cycle Savings
SH	Space Heating
SF	Solar Fraction

References

- Mehdaoui, F., Hazami, M., Messaouda, A., et al. "Performance analysis of two types of solar heating systems used in buildings under typical North-African climate (Tunisia)", *Appl. Therm Eng.*, **165**, p. 114203 (2020).
- Hazami, M., Mehdaoui, F., Naili, N., et al. "Energetic, exergetic and economic analysis of an innovative Solar CombiSystem (SCS) producing thermal and electric energies: Application in residential and tertiary households", *Energy Convers. Manag.*, **140**, pp. 36–50 (2017).
- Rey, A. and Zmeureanu, R. "Multi-objective optimization framework for the selection of configuration and equipment sizing of solar thermal combisystems", *Energy*, **145**(c), pp. 182–194 (2018).
- Katsaprakakis, D.A. and Zidianakis, G. "Optimized dimensioning and operation automation for a solar-combi system for indoor space heating. A case study for a school building in Crete", *Energies*, **12**, p. 177 (2019).
- Karami, M. and Javanmardi, F. "Performance assessment of a solar thermal combisystem in different climate zones", *Asian J. of Civil Eng.*, **21**, pp. 751–762 (2020).
- Englmair, G., Kong, W., Berg, J.B., et al. "Demonstration of a solar combi-system utilizing stable supercooling of sodium acetate trihydrate for heat storage", *Appl. Therm. Eng.*, **166**, p. 114647 (2020).
- Kannan, A., Prakash, J., and Roan, D. "Design and performance of an off-grid solar combisystem using phase change materials", *Int. J. of Heat Mass Trans.*, **164**, p. 120574 (2021).
- Thapa, B., Wang, W., and Williams, W. "Life-cycle cost optimization of a solar combisystem for residential buildings in Nepal", *J. of Asian Arch. Build. Eng.*, **21**(3), pp. 1137–1148 (2021).
- Meister, C. and Beausoleil-Morrison, I. "Experimental and modelled performance of a building-scalesolar thermal system with seasonal storage water tank", *Sol Energy*, **222**, pp. 145–159 (2021).
- Ahmadi, E., McLellan, B., Mohammadi-Ivatloo, B., et al. "The role of renewable energy resources in sustainability of water desalination as a potential freshwater source: An updated review", *Sustainability*, **12**, p. 5233 (2020).
- Asim, M., Uday Kumar, N.T., and Martin, A.R. "Feasibility analysis of solar combisystem for simultaneous production of pure drinking water via membrane distillation and domestic hot water for single-family villa: pilot plant setup in Dubai", *Desalin. Water Treat.*, **57**(46), pp. 21674–21684 (2016).
- Asim, M., Imran, M., Leunga, M.K.H., et al. "Experimental analysis of solar thermal integrated MD system for cogeneration of drinking water and hot water for single family villa in Dubai using flat plate and evacuated tube solar collectors", *Desalin. Water Treat.*, **92**, pp. 46–59 (2017).
- Asim, M. "Cogeneration of desalinated water and domestic hot water using membrane distillation technique for a family villa in the gulf region", *Physic. and Comput. Sciences*, **54**(4), pp. 397–409 (2017).
- Calise, F., d'Accadia, M.D., Vanoli, R., et al. "Transient analysis of solar polygeneration systems including seawater desalination: A comparison between linear Fresnel and evacuated solar collectors", *Energy*, **172**, pp. 647–660 (2019).
- Calise, F., Cappiello, F.L., Vicidominia, M., et al. "Water-energy nexus: A thermoeconomic analysis of polygeneration systems for small Mediterranean islands", *Energy Convers. Manage.*, **220**, p. 113043 (2020).
- Kumar, N.T.U. and Martin, A.R. "Co-production performance evaluation of a novel solar combi system for simultaneous pure water and hot water supply in urban households of UAE", *Energies*, **10**(4) (2017).
- Tariq, R., Sheikh, N.D., Xamanc, J., et al. "An innovative air saturator for humidification-dehumidification desalination application", *Appl. Energy*, **228**, pp. 789–807 (2018).
- Rahimi-Ahar, Z., Hatamipour, M.S., Ghalavand, Y., et al. "Comprehensive study on vacuum humidification-dehumidification (VHDH) desalination", *Appl. Therm. Eng.*, **169**, p. 114944 (2020).
- Zhao, Y., Zheng, H., Liang, S., et al. "Experimental research on four-stage cross flow humidification dehumidification (HDH) solar desalination system with direct contact dehumidifiers", *Desalin.*, **467**, pp. 147–157 (2019).

20. Rajaseenivasan, T. and Srithar, K. “Potential of a dual purpose solar collector on humidification dehumidification desalination system”, *Desalin.*, **404**, pp. 35–40 (2017).
21. Gabrielli, P., Gazzani, M., Novati, N., et al. “Combined water desalination and electricity generation through a humidification-dehumidification process integrated with photovoltaic-thermal modules: Design, performance analysis and techno-economic assessment”, *Energy Convers. Manag.* **X**, **1**, p. 100004 (2019).
22. Karami, M., Bozorgi, M., and Delfani, S. “Effect of design and operating parameters on thermal performance of low-temperature direct absorption solar collectors: a review”, *J. Therm. Anal. Calorim.* (2020).
23. Antoniadis, C.N. and Martinopoulos, G. “Optimization of a building integrated solar thermal system with seasonal storage using TRNSYS”, *Renew. Energy*, **137**, pp. 56–66 (2019).
24. Lenert, A. and Wang, E.N. “Optimization of nanofluid volumetric receivers for solar thermal energy conversion”, *Sol. Energy*, **86**, pp. 253–265 (2012).
25. Esmaili, M., Karami, M., and Delfani, S. “Performance enhancement of a direct absorption solar collector using copper oxide porous foam and nanofluid”, *Int. J. of Energy Research* (2020).
26. Delfani, S., Karami, M., and Akhavan Bahabadi, M.A. “Performance characteristics of a residential-type direct absorption solar collector using MWCNT nanofluid”, *Renew. Energy*, **87**, pp. 754–764 (2016).
27. Duffie, J.A. (Deceased), Beckman, W.A., and Blair, N., *Solar Engineering of Thermal Processes, Photovoltaics and Wind*, 5th Edn., Wiley (2020).
28. Patankar, A. “Numerical heat transfer and fluid flow”, *Computational Methods in Mechanics & Thermal Sciences*, CRC Press, 1st Edn. (1980).
29. Karami, M., Asghari, B., Delfani, S., et al. “Potential of nanodiamond/water nanofluid as working fluid of volumetric solar collectors”, *J. of Sol. Energy Research*, **2**(3), pp. 71–78 (2017).
30. Narayan, G.P., Sharqawy, M.H., Lienhard, V., et al. “Thermodynamic analysis of humidification dehumidification desalination cycles”, *Desalin. Water Treat.*, **16**(1–3), pp. 339–353 (2010).
31. Nawayseh, N.K., Farid, M.M., Omar, A.A., et al. “Solar desalination based on humidification process - II. Computer simulation”, *Energy Convers. Manag.*, **40**(13), pp. 1441–1461 (1999).
32. Iranian National Building Code, Part 16: Sanitary Installations (2017).
33. Kalogirou, S.A., *Solar Energy Engineering: Processes and Systems*, Second Ed., Elsevier Inc. (2014).
34. <https://www.alibaba.com>
35. Otanicar, T.P. and Golden, J.S. “Comparative environmental and economic analysis of conventional and nanofluid”, *Environ. Sci. Technol.*, **43**, pp. 6082–6087 (2009).
36. Central Bank of the Islamic Republic of Iran.
37. Tyra, B. “Electric power monthly with data”, *U.S. Energy Inf. Adm.*, pp. 1–772 (2019).
38. Rahaman, M.M. and Ahmed, T.S. “Affordable water pricing for slums dwellers in Dhaka metropolitan area: The case of three slums”, *J. Water Resour. Eng. Manag.*, **3**(1), pp. 15–33 (2016).

Biographies

Maryam Karami received her BS (2004) and PhD (2015) in Mechanical Engineering from the University of Tehran, Iran, and MS (2007) from Tarbiat Modares University, Tehran, Iran. Her specific research interest is renewable energy systems, HVAC systems, and building performance simulation. She has three books and numerous professional journal papers. She is currently working as an Assistant Professor in the Faculty of Engineering at Kharazmi University, Iran. Currently, more than 7 MS research students are working under his supervision.

Seyedeh Somayeh Nasiri Gahraz received her BS in Mechanical Engineering from Semnan University, Semnan, Iran, in 2017, and MS in Mechanical Engineering from Kharazmi University, Tehran, Iran, in 2020. Her research interests include water desalination, solar thermal systems, and dynamic simulation.